Journal of
Applied Crystallography
ISSN 0021-8898

Received 16 August 2006
Accepted 12 January 2007

The application of distance distribution functions to structural analysis of core–shell particles

Oleksandr O. Mykhaylyk,[a]* Anthony J. Ryan,[a] Nadezhda Tzokova[a] and Neal Williams[b]

[a]Department of Chemistry, University of Sheffield, Sheffield, S3 7HF, UK, and [b]ICI Paints, Wexham Road, Slough, Berkshire, SL2 5DS, UK. Correspondence e-mail: o.mykhaylyk@shef.ac.uk

The structure of core–shell latex particles of polymethylmethacrylate (the core) and polyurethane (the shell) have been investigated by methods of small-angle X-ray scattering (SAXS) and atom-force microscopy. A set of SAXS patterns has been obtained using contrast variation method. Indirect methods have been used to follow the evolution of distance distribution functions from SAXS for lattices in various sucrose solutions over a range of solution density, yielding structural parameters of the particles such as core size, shell thickness and density of the polymers including density deviations within the particle's core and shell. A model for an ensemble of core–shell particles with a normal distribution of average electron density of both the core and the shell has been developed to fit the distance distribution functions using a random search algorithm. The effects of nanophase separation in the polyurethane is estimated using Monte Carlo simulations of the distance distribution functions where the phase-separated polyurethane is represented by spherical truncated cones in a shell simulating the location of hard and soft polyurethane blocks, respectively.

1. Introduction

In general, most of objects of colloidal size (300–5000 Å) existing in nature could be classified as a core–shell formation comprising of a bulk body, which can be defined as a core, and a surface layer, defined as a shell, which is usually formed as a result of interaction between the body and the surrounding medium and functioning as a protecting barrier between the body and the rest of the world. Amongst these objects a dominating position is occupied by core–shell particles with spherical-like symmetry represented, for example, by vesicles (Discher & Eisenberg, 2002), liposome (Baumgart *et al.*, 2003), micelles (Hamley, 1998), latex particles (Bolze *et al.*, 2003) and viruses (Lin *et al.*, 1999). Two different approaches are usually used in structural characterization of the core–shell particles: microscopy (electron, scanning and atom-force) and scattering (dynamic light, neutron and X-ray). In spite of the fact that microscopy techniques are effective in the imaging of a real-space structure of matter, there is often an advantage in the application of scattering techniques, not least because they integrate over a large number of particles essentially performing an ensemble average; furthermore, scattering is non-destructive and simple to apply to studies of dynamic and kinetic processes.

Over the last twenty years it has been shown that small-angle X-ray scattering (SAXS) is a highly informative method for characterizing the structure of inhomogeneous particles to which core–shell formations are related. SAXS data from systems containing inhomogeneous particles can be treated assuming a model describing the particle shape and their internal structure. The form factor for various inhomogeneous particles, such as spherical, elliptical, cylindrical and sphero-cylindrical concentric shells with different scattering density are available in a full- or semi-analytical form (Pedersen, 1997). However, the difficulties in the interpretation of scattering functions obtained from experiment are caused by the highly abstract nature of reciprocal space. Serious progress in SAXS analysis has been made by the development of indirect methods where SAXS patterns available from experiment in only a limited region of scattering vectors are used to calculate the distance distribution function of particles $p(r)$ (Glatter, 1977; Svergun *et al.*, 1988).

The main advantage of distance distribution functions over scattering functions in interpretation of SAXS results is their representation of a structure in real space. If the shapes of inhomogeneous objects are known then $p(r)$ can be effectively used to study the inner structure of the objects. Inhomogeneous particles with at least two regions of electron densities differing in their sign, with respect to the scattering medium, show typical features in the distance distribution (Glatter, 1979). In this work, a set of distance distribution functions calculated from the SAXS patterns of latex core–shell particles obtained by the contrast variation method (Bolze *et al.*, 2003; Stuhrmann, 1982) have been analysed to demonstrate the effectiveness of $p(r)$ functions in an interpretation of the inner structure of core–shell particles.

2. Materials and methods

A set of samples of core–shell latex particles of polymethylmethacrylate (PMMA) and polyurethane (PU) of various sizes (in a range of 25–90 nm) have been synthesized by mini-emulsion polymerization of methylmethacrylate in a self-emulsifying dispersion of polyurethane (Gilbert, 1995). Atomic force microscopy (AFM) measurements (Veeco Instrument's Nanoscope III used in a tapping mode) obtained from very dilute aqueous solutions of colloidal particles (<1 wt% of polymer) dip-coated on a silicon wafer have shown spherical shape of the particles and have confirmed the

core–shell structure of the particles revealing the harder PMMA polymer was located in the core surrounded by the softer PU shell (Fig. 1*a*).

SAXS patterns were recorded at the Synchrotron Radiation Source, CCLRC Daresbury Laboratory, UK, on station 16.1 (wavelength of X-ray radiation $\lambda = 1.41$ Å, camera length 6 m) in a q-range of 0.008–0.07 Å^{-1} (the modulus of the scattering vector $q = 4\pi\sin\theta/\lambda$, where θ is a half of scattering angle) using a RAPID two-dimensional area detector. All measurements were carried out at room temperature. A liquid cell comprised of two mica windows (each of 25 µm thickness) separated by a polytetrafluoroethylene spacer of 1 mm thickness was used as a sample holder. Peak positions of a wet rat-tail collagen were used to calibrate the q-axis of the SAXS patterns. Two-dimensional SAXS patterns were reduced to one-dimensional profiles by a standard procedure available in the *BSL* software package (Bordas & Mant, 1996). The two-dimensional patterns, or their corresponding one-dimensional profiles, were subjected to incident beam intensity and background corrections. A smearing effect caused by the shape of the X-ray beam was corrected during the analysis using a profile of the direct beam recorded at the same setup of the station.

Preliminary SAXS studies of samples of the latex particles diluted in a water solution suggested that the sample containing particles of 70 nm in diameter had the lowest polydispersity. Thus, this sample was chosen for detailed investigations of the core–shell structure of the latex particles using the contrast variation method.

The total polymer content of the, as synthesized, colloidal suspension has been determined gravimetrically to be 40.2 wt%. The average mass density of the latex particles was determined to be 1.135 g cm^{-3} (the mass density has been measured for dried polymer films using a AccuPyc 1330V2.01 picnometer). These data have been used to prepare a set of colloids with a constant volume fraction of the latex particles (2 vol%) diluted in various water sucrose solutions (with mass density in a range 1.0–1.18 g cm^{-3}) to carry out SAXS measurements using the contrast variation method. The electron density of the aqueous medium was raised by adding certain amounts of D(+)-sucrose (Fluka, 98 wt%). Two sets of water sucrose solutions have been prepared: one set for dilution of the as-synthesized suspension compensating for the water in the sample following synthesis and another set for background subtraction to remove the solvent background from the experimental SAXS patterns of the colloids. The mass density of the water sucrose solutions agreed with those reported previously (Bolze *et al.*, 2003; Bubnik *et al.*, 1995). The linear relation between the electron density of a sucrose solution (ξ_m, defined in e Å^{-3}) and its mass density (ρ_m, defined in g cm^{-3}) (Bolze *et al.*, 2003) has been used in this work to evaluate electron densities of sucrose solutions.

In the analysis of the experimental SAXS patterns, distance distribution functions have been calculated using a regularization technique realised in the computer program *GNOM* (Svergun, 1992; Svergun *et al.*, 1988). The $p(r)$ functions for lattices dissolved in various sucrose solutions have been used in a further analysis to determine structural parameters of the particles such as the core size, the shell thickness and the density of the comprising polymers. An open source program *Dyefe* (Griffiths *et al.*, 1999; Nerukh, 2003) has been explored to fit the distance distribution functions using analytical expressions for different core–shell structure models discussed in this work. The program incorporates both simplex and random search algorithms which are stable and effective for problems with a number of parameters.

3. Results and discussion

The scattering intensities of the latex particles dissolved in solutions of varying contrast show from three to four minima (Fig. 2) suggesting that the polydispersity of the particles size is no greater than 10%. The twelve different contrasts created by water sucrose solutions with mass density in a range about 1.0–1.18 g cm^{-3} (or electron density in between 0.334 e Å^{-3} and 0.388 e Å^{-3}) include the average density of the polymers (1.135 g cm^{-3}). As could be expected for latex particles with a core–shell structure (Bolze *et al.*, 2003) the SAXS patterns exhibit a continuous shift of the minima towards bigger q values on increase of the density of the solution.

The shift in q of the first (and subsequent) minima observed in SAXS patterns from particles suspended in higher density solvent compared with lattices diluted in water (Fig. 2, mass density $\simeq$

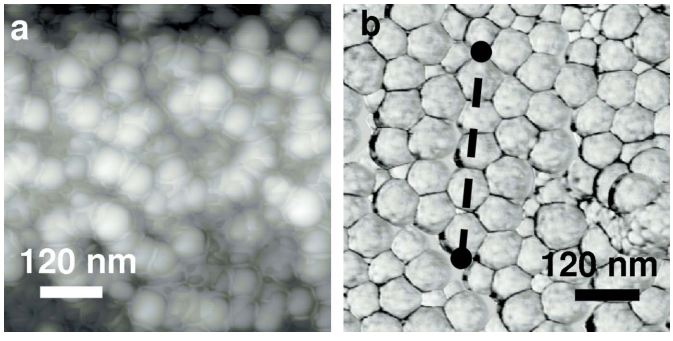

Figure 1
A representative AFM topographic image (*a*) of latex PU/PMMA particles dip coated on a silicon wafer surface, amplitude of the AFM tip vibrations has been tuned to detect the morphology (core–shell structure) of the particles, and (*b*) of a monolayer of latex PU/PMMA particles spin coated on a silicon wafer surface at 2000 rpm from dilute water solution (<0.1 wt% of polymer), the diameter of the particles averaged along the dashed line is about 740 Å.

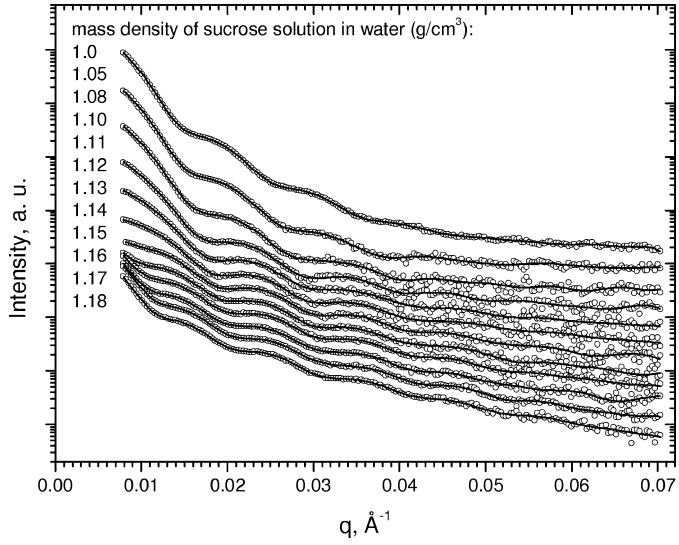

Figure 2
Experimental SAXS patterns of the PU/PMMA core–shell particles suspended in water sucrose solutions (2 vol.%) (circles) and corresponding scattering intensities restored by regularization technique using *GNOM* (solid lines). For ease of viewing each pattern has been normalized by coefficient 2^n, where n corresponds to the order of the pattern from the top to the bottom of the graph. Mass densities of the contrast solutions presented on the left-hand side of the graph follow in the order of the corresponding SAXS patterns.

1.0 g cm^{-3}) was followed by the appearance of a new minimum noticeable in SAXS pattern recorded for the lattices diluted in sucrose solution with mass density >1.15 g cm^{-3}.

The first minimum in SAXS patterns registered for the latex particles dissolved in contrasts with higher density tends towards the position of the first minima observed in SAXS for the lattices dissolved in water. This observation suggests that both the latex in pure water solution and the latex in high-density sucrose solution (1.18 g cm^{-3} or higher) correspond to two opposite cases: dense particles in a less-dense solution or less-dense particles in a dense solution. In both of these cases the structural inhomogeneities of the spherical core–shell particles could be neglected and the observed SAXS patterns could be interpreted as scattering from homogeneous spherical particles.

The indirect Fourier transformation method has been applied assuming that the analysed objects have a spherical symmetry and the distance distribution function $p(r)$ differs from zero only in the interval $0 \leq r \leq 850$ Å. In all cases, the parameter TOTAL, used in the program *GNOM* as the main criteria for the determination of the optimum value of the regularization parameter (Lagrange multiplier), was in between 0.7 and 0.91, suggesting either a reasonable or a good solution.

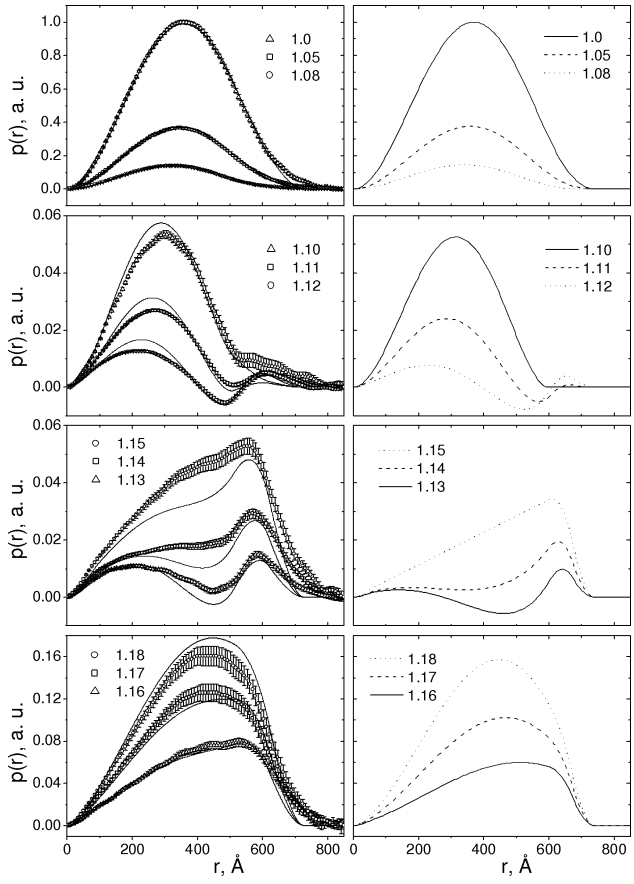

Figure 3
Distance distribution functions obtained by indirect method from experimental SAXS patterns of PU/PMMA latex particles presented in the Fig. 2 (left-hand side column of the plots) and compared with those calculated for the model core–shell particles (R_c = 300 Å, R = 370 Å, ξ_c = 0.379 e Å^{-3} and ξ_s = 0.364 e Å^{-3}) surrounded by different contrast media (right-hand side column of the plots). Figures on the plots indicate mass density (in g cm^{-3}) of the corresponding sucrose solution. Both experimental and simulated sets of distance distribution functions have been normalized by the maximum value obtained in its own $p(r)$ corresponding to the latex particles diluted in water ($\rho_m \simeq 1.0$ g cm^{-3}). The distance distribution functions obtained from the experiment have been fitted with the equation of $p(r)$ corresponding to the ensemble of core–shell particles with normal distribution of electron densities of both the core and the shell, equation (1) (the obtained parameters are: R_c = 258 Å, R = 365 Å, ξ_c = 0.381 e Å^{-3}, ξ_s = 0.366 e Å^{-3}, σ_c = 0.017 e Å^{-3} and σ_s = 0.005 e Å^{-3}). The model and the parameters are discussed later in the text.

The set of distance distribution functions, from latex PU/PMMA particles dissolved in a matrix of sucrose solutions with different electron densities, demonstrates (Fig. 3, left-hand side) all the features that could be expected for particles with a core–shell structure (Glatter, 1979) including all the special cases of matching the electron density of both the core and the shell. A qualitative analysis of the distance distribution functions shows that the latex in water (mass density about 1.0 g cm^{-3}) can be interpreted as a system of homogeneous spherical particles with a total radius (R) of about 370 Å. Indeed, a similar value can be found from AFM (Fig. 1*b*). This observation suggests that the electron density of the polymers located in both the core and the shell are significantly greater than the electron density of the water (taking into account the average density of the polymer). An increase in the electron density of the contrast solution ξ_m up to 0.364 e Å^{-3} (ρ_m = 1.10 g cm^{-3}) does not produce significant changes in the shape of the $p(r)$ (Fig. 3). The appearance of an oscillation with two pronounced peaks in the distance distribution function obtained for the lattices in sucrose solution with a higher density (ρ_m = 1.11 g cm^{-3}) suggests that one of the differences between the electron density of the medium and the core and between the medium and the shell has changed sign, that is, became positive. Following the evolution of the distance distribution functions it can be concluded, as suggested by the AFM results (Fig. 1*a*), that the electron density of the shell (ξ_s) is less than the electron density of the core (ξ_c) and the matching point of the electron density of the shell has been achieved by a contrast solution with ρ_m = 1.10 g cm^{-3} (Fig. 3). Thus, the scattering intensity produced by the lattices in such a solution should ideally correspond to scattering from the core only and the radius of the core (R_c) estimated from the corresponding distance distribution function is about 300 Å. A further increase of the electron density of the solutions lead to a disappearance of the oscillations in $p(r)$ producing a distance distribution function similar to that of a hollow sphere (Glatter, 1979) at a solution mass density of 1.15 g cm^{-3} (Fig. 3). Thus, the electron density of this sucrose solution (0.379 e Å^{-3}) can be interpreted as a matching point of the electron density of the core where the X-ray scattering should come from the shell only.

Substituting the estimated parameters (R = 370 Å, R_c = 300 Å, ξ_s = 0.364 e Å^{-3} and ξ_c = 0.379 e Å^{-3}) into the analytical expression of the distance distribution function for a coaxial core–shell spherical particle model [$p_{cs}(r)$] (see the supplementary information[1]) the $p_{cs}(r)$ for different media can be obtained (Fig. 3, right-hand side). In principle, the model $p_{cs}(r)$ reproduces all the features observed in the distance distribution functions calculated from the experimental SAXS patterns (Fig. 3). A significant discrepancy is observed between the amplitude of the model $p_{cs}(r)$ and the experimental $p(r)$, typically a factor of two, for the lattices suspended in sucrose solutions with electron densities between matching points of the shell and the core, ρ_m = 1.10 g cm^{-3} and ρ_m = 1.15 g cm^{-3}, respectively. There is also a noticeable tail at large values of r, associated with the shell of the particles in the distance distribution function corresponding to the core structure (Fig. 3, contrast solution with ρ_m = 1.10 g cm^{-3}). Furthermore, there is a pronounced curvature instead of a straight slope at distances mostly associated with the core of the particles in

[1] Supplementary data for this paper are available from the IUCr electronic archives (Reference: KS6029). Services for accessing these data are described at the back of the journal.

the distance distribution function corresponding to the shell structure (Fig. 3, contrast solution with ρ_m = 1.15 g cm^{-3}). Assuming a size polydispersity of the latex particles to be about 10% the observed discrepancy, which would require about half of the volume of the latex particles to be spread over a wide region of particle sizes, cannot be totally associated with this effect.

Another possibility for interpretation of the observed discrepancy between the experimental and the model $p(r)$ functions is to consider electron density deviations in both the core and the shell of the particles. Indeed, the synthesis method used for the preparation of the core–shell particles controls both the initial polydispersity of the PU seed particles used for the formation of the core–shell particles and the total amount of methylmethacrylate dissolved in the seed PU particles forming the core prior to polymerization. It might be expected that the polymerization process, with these two parameters under control, will produce core–shell particles with a relatively narrow distribution of the total diameter, which is confirmed by SAXS measurements (Fig. 2). However, the spatial distribution of the different polymers within the particles themselves, which may form bubble-like morphologies in one another or even continuous interpenetrating networks, could be variable due to the stochastic nature of the mini-emulsion process, thereby changing the average electron density of the core and the shell from one particle to another. It has also to be noted that the polyurethane itself can phase separate into hard and soft blocks *via* spinodal decomposition (Hamley *et al.*, 2000), which makes an extra contribution to the electron density deviations, especially in the shell of the particles. Some evidence of PU phase separation can be found in the AFM image of this material (Fig. 1*b*),

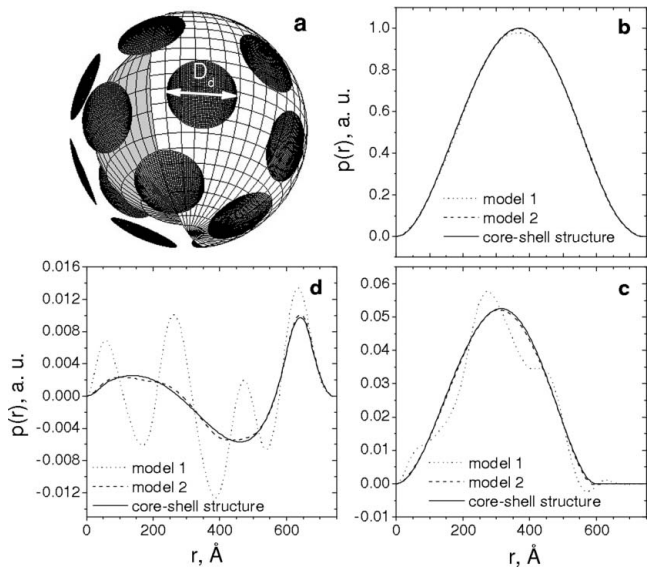

Figure 4
A model of the core–shell particle with spherical disks evenly distributed in the shell of the particle imitating phase separation of a polymer material in the shell (*a*) and distance distribution functions calculated for the model particle surrounded by different contrast media with mass density 1.0 g cm^{-3} (*b*), 1.10 g cm^{-3} (*c*) and 1.13 g cm^{-3} (*d*). Parameters of the models: model 1, R_c = 300 Å, R = 370 Å, diameter of the disks D_d = 200 Å, ρ_c = 1.15 g cm^{-3}, ρ_s = 1.0 g cm^{-3}, density of the disks ρ_d = 1.2 g cm^{-3}, the densities are present in mass density units of water sucrose solution, and number of the disks is 22, which corresponds to the ratio of the volume fraction of the disks and the rest of the shell as about 1:1; model 2, the same as above but ρ_s = 1.08 g cm^{-3} and ρ_d = 1.12 g cm^{-3} and the core–shell structure, R_c = 300 Å, R = 370 Å, ρ_c = 1.15 g cm^{-3}, ρ_s = 1.10 g cm^{-3}, no disks. For the sake of clarity the top surface of the disks and not the whole disks with the thickness of the shell is shown. Each set of distance distribution functions has been normalized by the maximum value obtained in $p(r)$ of the core–shell structure surrounded by a water solution ($\rho_m \simeq$ 1.0 g cm^{-3}).

where disk-like domains evenly distributed over the surface of the particles with inter-domain distances in a range 100–200 Å can be interpreted as an ordered phase-separated structure. Thus, two structural models for the core–shell particles have been considered. One model represents the system as core–shell particles with a phase separation in the shell and is called a model of spherical disks (Fig. 4*a*). The analysis of this model is presented as supplementary information. The simulations have shown (Fig. 4) that only well defined phase separation in the shell structure with significant difference in the electron densities of the phase-separated materials can be identified in the distance distribution functions obtained for latex particles.

A more likely model describes an ensemble of core–shell particles with a normal distribution of the average electron density of both the core and the shell (the model of normal electron density distribution). Because of the complexity of the calculations the model at this stage has only been considered for an ensemble of particles which are monodisperse in size. SAXS patterns corresponding to a dilute solution of an ensemble of particles can be considered as a linear superposition of scattering patterns generated by each particle of the ensemble. As the Fourier transformation is linear, $p(r)$ calculated from this pattern is the sum over all the distance distribution functions from each particle in the ensemble. Thus, $p(r)$ corresponding to the model of normal electron density distribution can be obtained as a double integration over probability distribution functions of electron densities of the core $P(\xi_c)$ and the shell $P(\xi_s)$ of the particles in the ensemble:

$$p(r) = \int_{\xi_{0c}-6\sigma_c}^{\xi_{0c}+6\sigma_c} P(\xi_c) \int_{\xi_{0s}-6\sigma_s}^{\xi_{0s}+6\sigma_s} P(\xi_s) p_{cs}(r, \xi_c, \xi_s) \mathrm{d}\xi_c \mathrm{d}\xi_s \qquad (1)$$

where $p(r,\xi_c,\xi_s)$ is the distance distribution function of a core–shell particle (see supplementary information) and $P(\xi) = a\exp[-(\xi - \xi_0)^2/$

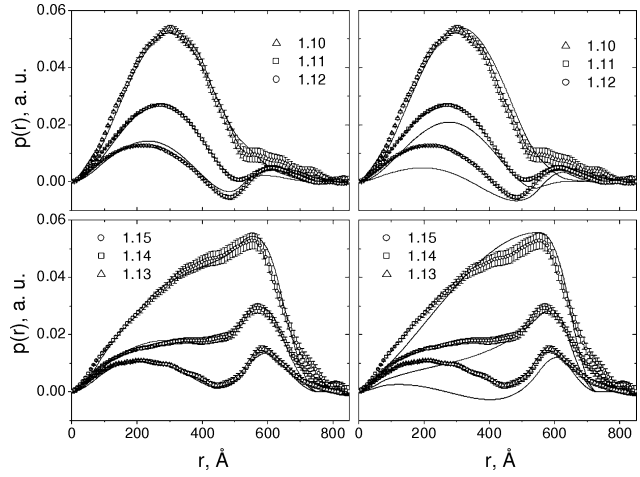

Figure 5
Distance distribution functions of the PU/PMMA latex particles suspended in various contrast sucrose solutions with electron densities in a range between the average electron density of the shell and the core of the particles fitted with the model of normal distribution of particles with variable electron densities, equation (1) (left-hand side, the obtained parameters are: R_c = 259 Å, R = 378 Å, ξ_c = 0.379 e Å^{-3}, ξ_s = 0.366 e Å^{-3}, σ_c = 0.018 e Å^{-3} and σ_s = 0.005 e Å^{-3}) and with the core–shell model, $p_{cs}(r)$ (right-hand side, the obtained parameters are: R_c = 277 Å, R = 366 Å, ξ_c = 0.377 e Å^{-3}, ξ_s = 0.366 e Å^{-3}). Numbers presented on each plot indicate mass density (in g cm^{-3}) of the corresponding contrast solutions. The distance distribution functions have been normalized by the maximum value obtained in $p(r)$ of the latex particles diluted in a water solution ($\rho_m \simeq$ 1.0 g cm^{-3}).

$(2\sigma^2)]$ is a normal (Gaussian) distribution function of electron density, ξ_0 and σ are the average electron density and the standard deviation, respectively, of either the core or the shell. It has been assumed in the equation (1) that both distribution functions $P(\xi_c)$ and $P(\xi_s)$ are independent of each other. To express the results of the integration analytically defined limits for the range of electron densities have been used which cover 99.9% of the distribution. The result of the integration has a very long analytical expression and is not presented herein; however, it can be obtained using a standard mathematical computer package (for example, *Maple* or *Mathematica*). The expression obtained has been incorporated into a computer program, *Dyefe*, and used to fit the distance distribution functions obtained from experimental SAXS patterns (Fig. 3, left-hand side).

An application of the equation (1) to the simultaneous fitting of all 12 distance distribution functions calculated from SAXS patterns shows a reasonable fit to the model (Fig. 3, left-hand side, solid lines) for the full range of contrast variation. The curves obtained reproduce all the features observed in $p(r)$ calculated from experimental data with some deviations in the amplitudes of the $p(r)$ corresponding to latex particles in sucrose solutions with ρ_m in a range between 1.10 and 1.15 g cm^{-3} matching electron densities of the shell and the core. It would be convenient to divide the $p(r)$ into two groups: a group at extremes of contrast containing the first three and the last three $p(r)$ (surrounding media ρ_m = 1.0–1.08 g cm^{-3} and 1.16–1.18 g cm^{-3}, respectively) and a group of intermediate $p(r)$ (surrounding media ρ_m = 1.10–1.15 g cm^{-3}). The $p(r)$ obtained at the extremes of solution density correspond to the case where the electron density contrast between the media and the particles is dominant and, therefore, the SAXS measurements are less sensitive to the internal structural peculiarities of the particles. The intermediate $p(r)$ correspond to the case where X-ray scattering mostly originates from electron density deviations within the particles, and is very sensitive to the internal structural morphology of the particles. The amplitudes of the $p(r)$ at extreme contrast are much higher (up to 100 times) than the amplitudes of $p(r)$ at intermediate contrast, thus, the parameters of the model obtained from the simultaneous fitting of both the extreme contrast $p(r)$ and the intermediate contrast $p(r)$ will be strongly dependent on the higher magnitude $p(r)$, which may cause some deviations in the fitting at intermediate contrast (Fig. 3, left-hand side column). To alleviate this numerical constraint in the fitting process either weighting coefficients have to be assigned to each distance distribution function used in the fitting or two groups of $p(r)$ functions have to be fitted independently. Indeed, a simultaneous fitting of the group of intermediate contrast $p(r)$ has produced curves closely following the original $p(r)$ functions calculated from experimental SAXS patterns (Fig. 5, left-hand side). The parameters of the model obtained from both fittings (Fig. 3 and Fig. 5) are quantitatively similar with some noticeable deviations in the total size of the particles R, where preference should be given to the result obtained from the fitting with the extreme contrast $p(r)$, which is more reliable for this parameter. It is also worth showing that fitting the group of the intermediate contrast $p(r)$ functions with the standard core–shell model $p_{cs}(r)$ produces a rather poor result (Fig. 5, right-hand side). Significant discrepancies between the fitted curves and the $p(r)$, especially in the core region ($r \simeq 300$ Å), which cannot be improved by this model *a priori*, once again demonstrate the strong effect of electron density deviations in the modelling of SAXS results.

Two other effects that are likely to produce the deviations between the curves obtained from the simultaneous fitting of all 12 $p(r)$ functions (Fig. 3) are a polydispersity in the total particle radius R and a polydispersity in the core radius R_c, neither of which have been taken account of in the model. The latter may be caused by a random distribution of some PMMA in the PU-rich shell and some PU in the PMMA-rich core constrained by a fixed PU/PMMA ratio in the particle. In this case the assumption of independent distribution functions $P(\xi_c)$ and $P(\xi_s)$ taken in the model of normal distribution of electron densities [equation (1)] is no longer valid. The introduction of polydispersity functions of both the core radius and the total radius of the particles in the model can, however, significantly complicate the fitting procedure.

In spite of neglecting the size polydispersity the model has produced a good fit to the distance distribution functions calculated from SAXS measurements with reasonable parameters. The total diameter of the particles (730 Å) is consistent with the value measured from AFM images (740 Å, Fig. 1*b*). The average mass density of the core ρ_c = 1.165 g cm^{-3} calculated from the average electron density ξ_c = 0.379 e Å^{-3} [$\rho = \xi M/z/N_A$, where $M \simeq 100$ and $z \simeq 54$ are the molecular weight and the number of electrons per molecular repeat unit for the PMMA and N_A is Avogadro's number (Bolze *et al.*, 2003)] is in a good agreement with the mass density of PMMA 1.17–1.20 g cm^{-3} (Mark, 1999). Similar calculations made to estimate the average mass density of the polyurethane shell produced ρ_s = 1.110 g cm^{-3} (ξ_s = 0.366 e Å^{-3}, M/z = 1.826), which is close to the mass density measured for a dried polymer film comprising of the polyurethane only (1.104 g cm^{-3}). The fitting has also shown that the deviations of the average electron densities of the core (σ_c = 0.063 e Å^{-3}) are a few times higher than the deviations in the shell (σ_s = 0.018 e Å^{-3}) of the particles. This may be a feature of the nano-phase separation that takes place when the acrylic is polymerized. Prior to polymerization the particles comprise a homogeneous polyurethane particle swollen with MMA monomer, polymerization causes phase separation between the PU and PMMA with the PU segregating predominantly to the surface, however, some PU could be trapped in the interior of the particle due to vitrification of the PMMA leading to a higher variation in electron density in the core. Using the mass density of the polymers and geometrical parameters of the core and the shell measured from SAXS, the average density of the polymers can be obtained as 1.130 g cm^{-3} which is in a good agreement with the total density of a dried polymer film (1.135 g cm^{-3}) associated with the average density of the latex particles.

4. Conclusions

The internal structure of core–shell particles has been studied using SAXS with the method of contrast variation. The indirect Fourier transform yielded distance distribution functions that were compared with three models of increasing sophistication: simple core–shell, core–shell with spherical disks and core–shell with stochastic electron density variations. Rather than fitting the scattering intensity the real-space models of particle density have been applied directly to the distance distribution functions. Parameters were extracted from both the simple core–shell and the core–shell with stochastic density variations by a simultaneous fitting of the full set and sub-sets of the distance distribution functions corresponding to different contrasts. The real density of the core and shell were predicted well by the average density from both models. The simple core–shell model was in good agreement with both the qualitative shape of the distance distribution functions and its amplitude when the electron density of the medium was very different to that of the particles, but failed to describe the amplitude of the distance distribution functions when the density of the medium was close to, or matched that, of either core or shell. Both the shape and amplitude of the distance distri-

bution function could be described by a stochastic density variation model that indicated that there were local variations in density that could have a Gaussian distribution over the particles with a greater variation in the density of the core than that of the shell. This is consistent with the preparation method where polymerization is initiated in an ensemble of particles that represent a distribution of slightly different initial states and proceed to a stochastic distribution of final states by constrained phase separation.

OOM is grateful for EPSRC funding under grant GR/T11852/01. Both OOM and NT thank ICI for postdoctoral fellowships. The authors also thank the SRS, Daresbury Laboratory, for beamtime for the SAXS experiments.

References

Baumgart, T., Hess, S. T. & Webb, W. W. (2003). *Nature*, **425**, 821–824.
Bolze, J., Ballauff, M., Kijlstra, J. & Rudhardt, D. (2003). *Macromol. Mater. Eng.* **288**, 495–502.
Bordas, J. & Mant, G. (1996). *BSL*, http://www.ccp13.ac.uk/software/oschoice.html.
Bubnik, Z., Kadlec, P., Urban, D. & Bruhns, M. (1995). *Sugar Technologists Manual*. Berlin: Bartens.
Dischер, D. E. & Eisenberg, A. (2002). *Science*, **297**, 967–973.
Gilbert, R. G. (1995). *Emulsion Polymerization*. London: Academic Press.
Glatter, O. (1977). *J. Appl. Cryst.* **10**, 415–421.
Glatter, O. (1979). *J. Appl. Cryst.* **12**, 166–175.
Griffiths, T. R., Nerukh, D. A. & Eremenko, S. A. (1999). *Phys. Chem. Chem. Phys.* **1**, 3199–3208.
Hamley, I. W. (1998). *The Physics of Block Copolymers*. Oxford: Oxford University Press.
Hamley, I. W., Stanford, J. L., Wilkinson, A. N., Elwell, M. J. & Ryan, A. J. (2000). *Polymer*, **41**, 2569–2576.
Lin, T., Chen, Z., Usha, R., Stauffacher, C. V., Dai, J. B., Schmidt, T. & Johnson, J. E. (1999). *Virology*, **265**, 20–34.
Mark, J. E. (1999). Editor. *Polymer Data Handbook*. Oxford: Oxford University Press.
Nerukh, D. A. (2003). *Dyefe-Dynamic Equation Fitting Engine*, http://www.chem.pwf.cam.ac.uk/~dn232/software/dyefe/index.html.
Pedersen, J. S. (1997). *Adv. Colloid Interface Sci.* **70**, 171–210.
Stuhrmann, H. B. (1982). *Small Angle X-ray Scattering*, edited by O. Glatter & O. Kratky, pp. 197–213. London: Academic Press.
Svergun, D. I. (1992). *J. Appl. Cryst.* **25**, 495–503.
Svergun, D. I., Semenyuk, A. V. & Feigin, L. A. (1988). *Acta Cryst.* A**44**, 244–250.